Journal of Power Sources 263 (2014) 181–185

Contents lists available at ScienceDirect

Journal of Power Sources

journal homepage: www.elsevier.com/locate/jpowsour

Short communication

Graphene film-confined molybdenum sulfide nanoparticles: Facile one-step electrodeposition preparation and application as a highly active hydrogen evolution reaction electrocatalyst

Zonghua Pu [a], Qian Liu [a], Abdullah M. Asiri [b,c], Abdullah Y. Obaid [b,c], Xuping Sun [a,b,c,*]

[a] Chemical Synthesis and Pollution Control Key Laboratory of Sichuan Province, School of Chemistry and Chemical Industry, China West Normal University, Nanchong 637002, Sichuan, China
[b] Chemistry Department, Faculty of Science, King Abdulaziz University, Jeddah 21589, Saudi Arabia
[c] Center of Excellence for Advanced Materials Research, King Abdulaziz University, Jeddah 21589, Saudi Arabia

HIGHLIGHTS

- We demonstrate the first one-step fabrication of graphene film-confined MoS_x nanoparticles.
- Such hybrid film is used as a novel HER electrocatalyst in acidic solution.
- Such hybrid film shows high HER activity and good stability.

ARTICLE INFO

Article history:
Received 24 January 2014
Received in revised form
18 March 2014
Accepted 20 March 2014
Available online 24 April 2014

Keywords:
One-step electrodeposition
Graphene
Molybdenum disulfide
Hydrogen evolution reaction

ABSTRACT

MoS_x nanoparticles–graphene hybrid film was deposited onto a glassy carbon electrode by a facile one-step electrodeposition approach using MoS_4^{2-} and graphene oxide as precursors. As a novel hydrogen evolution reaction (HER) electrocatalyst, this hybrid film exhibits highly catalytic activity and good stability.

1. Introduction

Hydrogen is an ideal candidate for the replacement of fossile fuels in the future [1]. Electrolysis of water, currently the simplest way to produce hydrogen of high purity at the most economical price, has attracted considerable attention [2,3]. The noble metals, such as platinum, have large cathodic current densities at low overpotentials in the hydrogen evolution reaction (HER) [4–6]. However, they suffer from high cost and resource scarcity, hindering their large-scale applications. Thus, replacement of Pt with earth-abundant metals is highly desirable.

Over the past few years, MoS_2 has been identified as promising alternatives for noble metals due to its earth abundance composition and excellent HER activity [7]. Both experimental and theoretical results suggest that the HER activity originates from the sulfur edges of MoS_2 layers, while the basal surfaces are catalytically inert [8–11]. Bulk MoS_2 shows poor HER activity [12], but such issue can be solved by designing MoS_2 nanostructures with more edge sites. The poor electrical conductivity issue of MoS_2 can be fixed by using conductive carbon as a support. Indeed, Dai and coworkers have developed reduced graphene oxide (GO) supported MoS_2 nanoparticles as highly efficient HER electrocatalysts [13]. For electrocatalytic application, the direct fabrication of catalyst film onto electrode surfaces has an obvious advantage of eliminating the immobilization step; however, the development of catalyst film based on MoS_2 for HER is scarcely reported. Until recently have Chang et al. deposited hydrothermally MoS_x onto graphene-protected three-dimensional Ni foams for highly efficient

* Corresponding author. Chemical Synthesis and Pollution Control Key Laboratory of Sichuan Province, School of Chemistry and Chemical Industry, China West Normal University, Nanchong 637002, Sichuan, China
E-mail addresses: sunxp@ciac.jl.cn, sun.xuping@hotmail.com (X. Sun).

http://dx.doi.org/10.1016/j.jpowsour.2014.03.093
0378-7753/

hydrogen production [14]; however, it suffers from the involvement of dangerous gases (H_2), high temperatures and a complicated procedure for catalyst film preparation.

In this communication, for the first time, we demonstrate the facile deposition of MoS_x nanoparticles–graphene (MoS_x–G) hybrid film onto a glassy carbon electrode (GCE) by a one-step electrodeposition approach with the use of MoS_4^{2-} and graphene oxide as precursors. We further show the utilization of such hybrid film as a highly active HER electrocatalyst with an overpotential of 200 mV at a cathodic current density of 17 mA cm^{-2}. A small Tafel slope of 43 mV dec^{-1} is observed, suggesting that the surface chemistry mechanism is responsible for HER. Such catalyst exhibits a good stability.

2. Experimental

2.1. Reagents and materials

H_2SO_4 was purchased from Tianjin Fuyu Chemical Reagent Co. Ltd., China. $(NH_4)_2MoS_4$ was purchased from Sinopharm Chemical Reagent Co., Ltd (Shanghai, China). Pt/C (20 wt% Pt on Vulcan XC-72R) was purchased from Sigma–Aldrich. All chemicals were used as received without further purification. The water used throughout all experiments was deionized water purified through a Millipore system.

2.2. Preparation of MoS_x–G hybrid film

The cyclic voltammograms (CVs) were performed for the electrochemical deposition of MoS_x–G hybrid film with the potential range from −1.2 V to 0.5 V with a scan rate of 30 mV s^{-1} for different scan cycles [15]. The deposition bath used for the electrodeposition was simply composed of $(NH_4)_2MoS_4$ (5 mM) and GO (1 mg mL^{-1}). GCE was used as working electrode for electrodeposition. A graphite electrode and an Ag/AgCl electrode were used as the counter electrode and reference electrode, respectively. For comparison, pure MoS_x was electrodeposited on GCE by the same route without adding GO into the deposition solution. The loading of MoS_x–G was about 0.1 mg cm^{-2}.

2.3. Structural characterizations

Scanning electron microscopy (SEM) images were taken on an XL30 ESEM. X-ray photoelectron spectroscopy (XPS) experiments were made on an ESCALABMK II X-ray photoelectron spectrometer using Mg as the exciting source.

2.4. Electrochemical characterization

Electrochemical measurements are performed with a CHI 660D electrochemical analyzer (CH Instruments, Inc., Shanghai). The electrochemical properties of the prepared electrocatalysts were studied in a standard three-electrode system. The MoS_x–G or MoS_x modified GCE was used as the working electrode, a saturated calomel electrode (SCE) was used as the reference electrode, and graphite as the counter electrode. Electrical impedance spectroscopy (EIS) was recorded under the following conditions: AC voltage amplitude 5 mV, frequency ranges 10^5–1 Hz.

3. Results and discussion

Fig. 1a shows the low-magnification scanning electron microscopy (SEM) image of the resulting hybrid film on GCE, indicating the film consists of a large amount of nanoparticles and graphene sheets. The high-magnification SEM image (Fig. 1b) further reveals the formation of MoS_x nanoparticles–graphene hybrid film. The deposition of graphene film from GO suspension can be rationally explained as follows [16]: GO in direct contact with GCE accepts electrons and is electrochemically reduced into graphene during cathodic scan. Because of their poor solubility in water, these graphene sheets are directly attached to GCE surface to form film. It is of importance to mention that electrodeposition without the presence of GO only produces film of pure molybdenum sulfide nanoparticles (Fig. 1c). The high-magnification SEM image (Fig. 1d) shows that the nanoparticles are nanoparticle aggregates or cross-linked nanoparticles. These results suggest that graphene film can effectively prevent the aggregation of the nanoparticles thus generated.

The chemical states of Mo and S in the hybrid film were further investigated by X-ray photoelectron spectroscopy (XPS). Fig. 2 displays the detailed XPS scans for the Mo and S binding energies for these MoS_x catalysts. The binding energies of Mo $3d_{5/2}$ and Mo $3d_{3/2}$ are 228.9 eV and 232.1 eV, respectively, which can be assigned to Mo^{4+} [17–19]. The peaks, corresponding to the S $2p_{1/2}$ and $2p_{3/2}$ orbitals of divalent sulfide ions (S^{2-}) are observed at 162.9 and 161.8 eV. The S: Mo stoichiometric ratio is 2.1, suggesting that the nanoparticle is close to MoS_2. In addition to the XPS peaks for MoS_2 structure, other sets of peaks are also observed. The observation of Mo $3d_{3/2}$ and Mo $3d_{5/2}$ binding energies at 233.1 and 230 eV suggests the presence of Mo^{5+} ions. The peak at 235.6 eV is that for $3d_{3/2}$ of Mo^{6+} [20]. The peak at 226.3 eV corresponds to the S 2s component [21]. Meanwhile, the S $2p_{1/2}$ and S $2p_{3/2}$ energies at 164.3 and 163.2 eV indicate the existence of bridging S_2^{2-} or apical S^{2-} [22,23]. The S 2p spectrum can be fit with two S 2p doublets, which is similar to those of amorphous MoS_3. These observations imply the coexistence of MoS_2 and MoS_3 [24].

The MoS_x–G hybrid film is prepared by CVs with the potential range from −1.2 V to 0.5 V with a scan rate of 30 mV s^{-1} for 30 scan cycles, as shown in Fig. 3a. Electrochemical measurements of the hybrid film were conducted in a three-electrode cell. The linear scan voltammograms (LSVs) measurements were used to test HER properties of MoS_x–G hybrid film and MoS_x film with a scan rate of 5 mV s^{-1} in 0.5 M H_2SO_4. Meanwhile, the commercial Pt/C catalyst was also tested with the same measurements. Fig. 3b shows the polarization curves of MoS_x–G, MoS_x and Pt/C. The MoS_x–G shows a small onset overpotential (η) of 130 mV for HER, which is smaller than that of MoS_x ($\eta = 160$ mV). And the Pt/C exhibits the best HER catalytic performance ($\eta = 20$ mV). Likewise, the highly catalytic activity is demonstrated by comparing the current density of MoS_x–G and MoS_x. For achieving a catalytic current density of 10 mA cm^{-2}, the overpotentials need to be 183 mV and 208 mV for MoS_x–G and MoS_x, respectively. Such performance of MoS_x–G is comparable to that of previous reports [7,9,24,25].

Tafel plots of these catalysts were recorded with the linear regions fitted into the Tafel equation ($\eta = a + b\log j$, where j is the current density and b is the Tafel slope) [26]. The Tafel slopes for Pt/C, MoS_x–G and MoS_x are ~30, ~43 and ~50 mV dec^{-1}, respectively (Fig. 3c).

In acid solutions, three principal reactions are assumed to predominate when hydrogen is evolved on a metal catalyst, commonly named the Volmer [Equation (1)], Heyrovsky [Equation (2)], and Tafel reactions [Equation (3)] [27].

$$H_3O^+ + e^- + \text{catalyst} \rightarrow \text{catalyst} - H + H_2O \quad (1)$$

$$H_3O^+ + e^- + \text{catalyst} - H \rightarrow \text{catalyst} + H_2 + H_2O \quad (2)$$

$$\text{catalyst} - H + \text{catalyst} - H \rightarrow 2\text{catalyst} + H_2 \quad (3)$$

The Tafel slope is an inherent property of the catalyst. When the Volmer reaction is the rate-determining step of the HER, Tafel

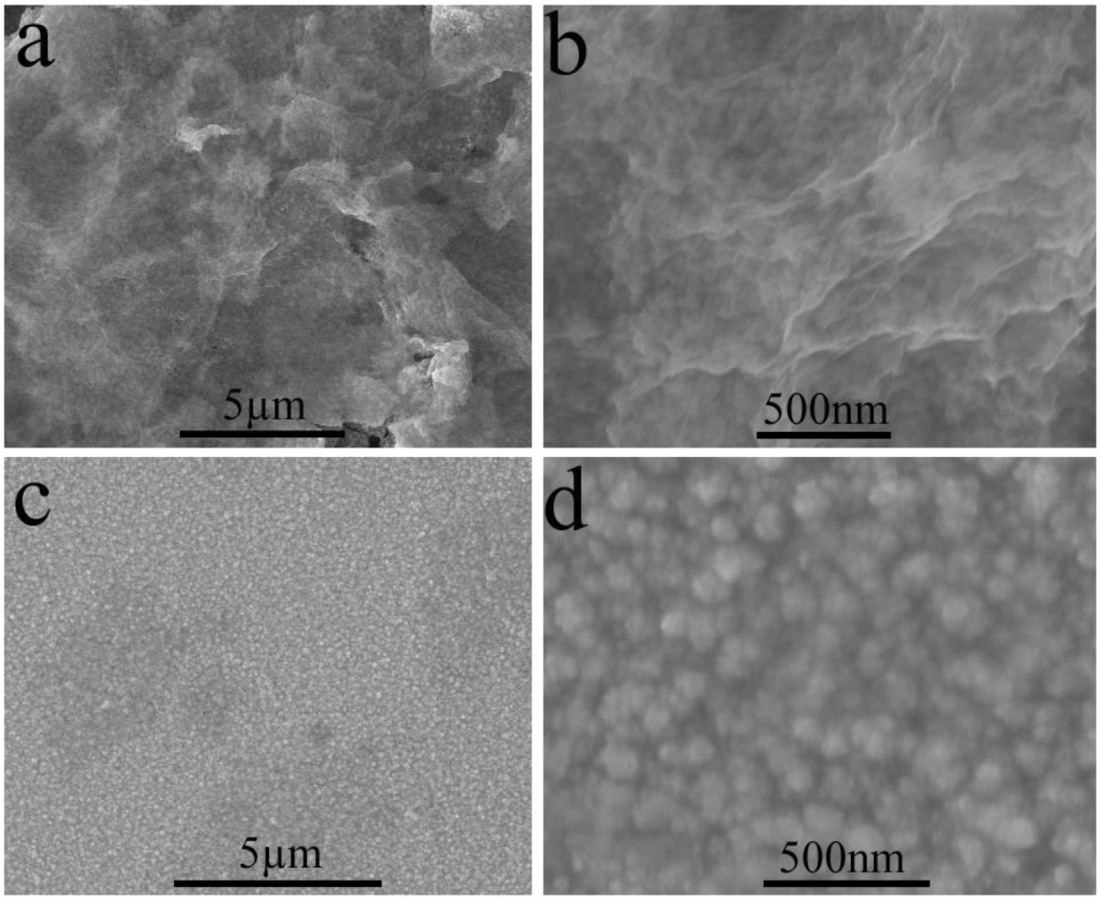

Fig. 1. (a) Low and (b) high magnification SEM images of electrodeposited hybrid film from MoS_4^{2-} and GO. (c) Low and (d) high magnification SEM images of electrodeposited film from MoS_4^{2-}.

slope ~120 mV dec^{-1}. Likewise, for the Heyrovsky or Tafel reaction, theoretical results should produce Tafel slopes of ~40 and ~30 mV dec^{-1}, respectively [28,29]. The observed Tafel slope of MoS_x–G (43 mV dec^{-1}) is a small value for an HER catalyst, suggesting that the surface chemistry mechanism is responsible for HER. And the Volmer–Heyrovsky HER mechanism is operative in the HER catalyzed by MoS_x–G [30].

To illustrate the relative enhancement of catalytic activity for MoS_x–G, the EIS data of MoS_x–G and MoS_x are shown in Fig. 3d. It is revealed that MoS_x–G shows a much smaller radius of semicircle in the Nyquist plots, compared with MoS_x, indicating the higher conductivity of MoS_x–G due to the presence of graphene. Also, the smaller Tafel slope and lower resistance correspond to a more favorable HER kinetics over MoS_x–G. The strong stability of catalyst is another vital issue to consider for commercial applications. We thus examined the durability of the MoS_x–G catalyst using CVs measurements for scanning 1000 cycles from −0.3 to −0.8 V vs. SCE with a scan rate of 100 mV s^{-1} in 0.5 M H_2SO_4. Fig. 3e shows that this catalyst has good stability in acidic electrolyte with slight anodic current loss after 1000 cycles. Also, different scan cycles

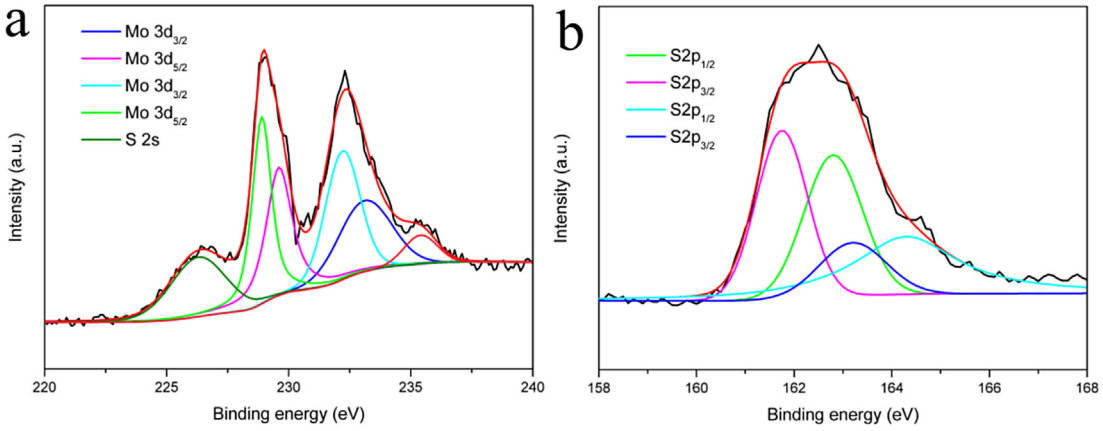

Fig. 2. XPS (a) Mo 3d and (b) S 2p spectrum.

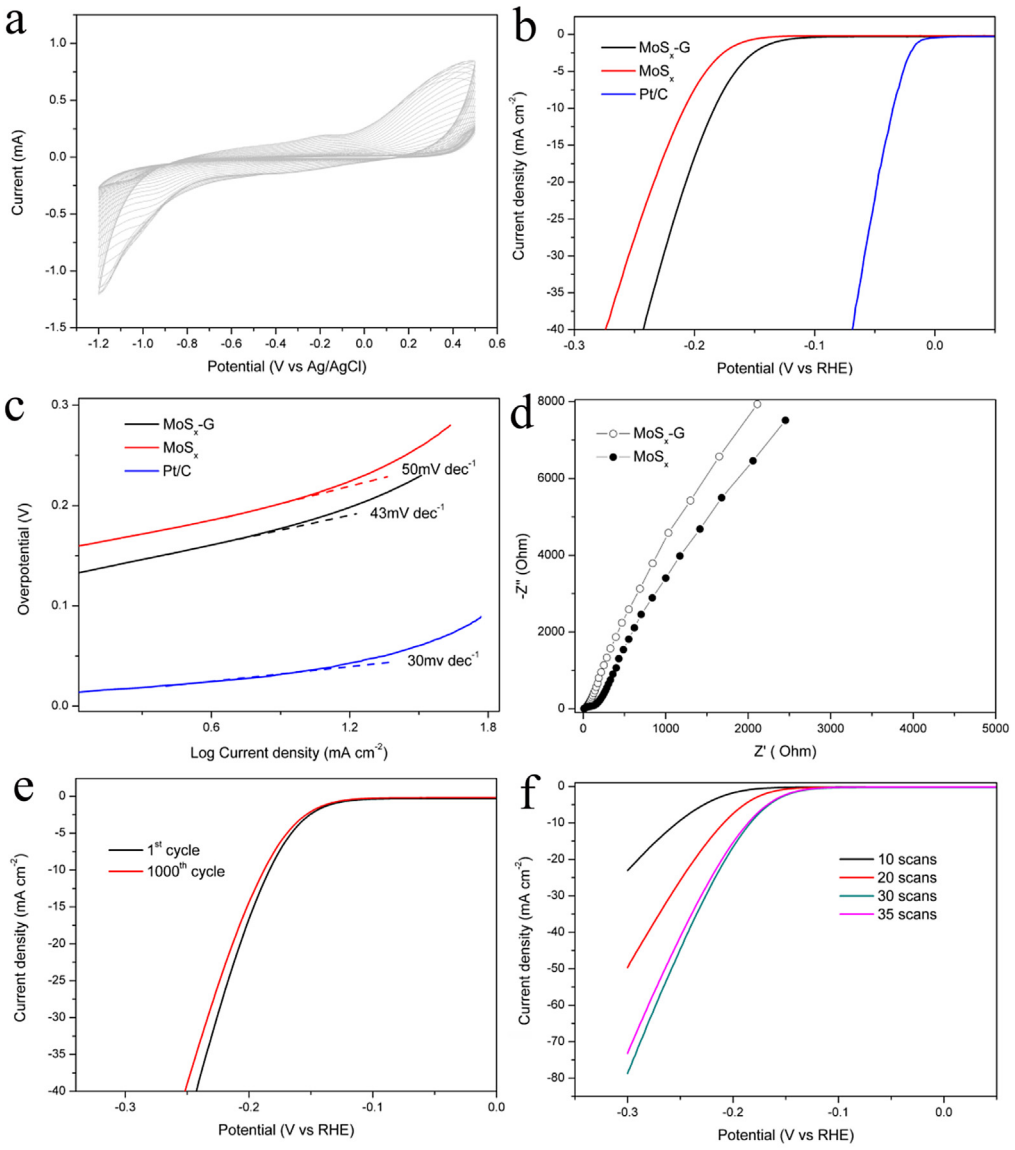

Fig. 3. (a) Deposition of MoS_x–G hybrid film on a GCE by repeated cyclic voltammetries (30 cycles). (b) Polarization curves of MoS_x–G, MoS_x and Pt/C in 0.5 M H_2SO_4 solution at a sweep rate of 5 mV s^{-1}. (c) Tafel plots of MoS_x–G, MoS_2 and Pt/C. (d) Nyquist plots of MoS_x–G and MoS_x. (e) Polarization curves of MoS_x–G before and after CV test of 1000 cycles. (f) Polarization curves for HER of MoS_x–G hybrid film made from different numbers of scanning cycles in 0.5 M H_2SO_4 solution with a sweep rate of 5 mV s^{-1}.

during the electrodeposition process were designed to investigate their effects on catalytic activity (Fig. 3f). In the initial 30 scan cycles, the HER activity of MoS_x–G increases with the number of scan cycles. However, at 35 scan cycles, the MoS_x–G shows lower HER activity, indicating that the catalytic activity approaches saturation with about 30 scans cycles.

The turnover frequency (TOF) of H_2 molecules evolved per second (represented as units of s^{-1}) for each active site was measured. The active sites were quantified by electrochemistry. When the number of active sites is known, TOF can be calculated with the following equation [24]:

$$\mathrm{TOF} = I/2Fn \tag{4}$$

where I is current (in A) during the linear sweep measurement, n is active sites number (in mol) and F is the Faraday constant (in C mol^{-1}). The factor 1/2 arrives by taking into account that two electrons are required to form one hydrogen molecule from two protons. CVs were recorded for these electrodes (MoS_x–G/GCE, MoS_x/GCE and bare GCE) with a scan rate of 50 mV s^{-1} in a pH = 7 phosphate buffer solution from −0.145 V to +0.655 V vs. RHE, as shown in Fig. 4a. Later, the absolute components of the voltammetric charges (cathodic and anodic) reported during one single blank measurement were added. Assuming a one electron redox process, this absolute charge was divided by two. The value was then divided by the Faraday constant to get the number of active sites of the film. Following this procedure, the number of active sites (in mol) was determined. The calculated TOFs for MoS_x–G and MoS_x in 0.5 M H_2SO_4 is shown in Fig. 4b. At $\eta = 250$ mV, a TOF of 2.27 s^{-1} was achieved for MoS_x which is lower than that derived for MoS_x–G (3.80 s^{-1}). These results indicate that MoS_x–G has better intrinsic catalytic activity. The higher catalytic performance of the hybrid film could be attributed to the following two reasons: (1) The conductive graphene film provides effective electron transport pathways for MoS_x; (2) MoS_x nanoparticles are strongly confined within graphene film, leading to unique structure with good stability and integrity [31].

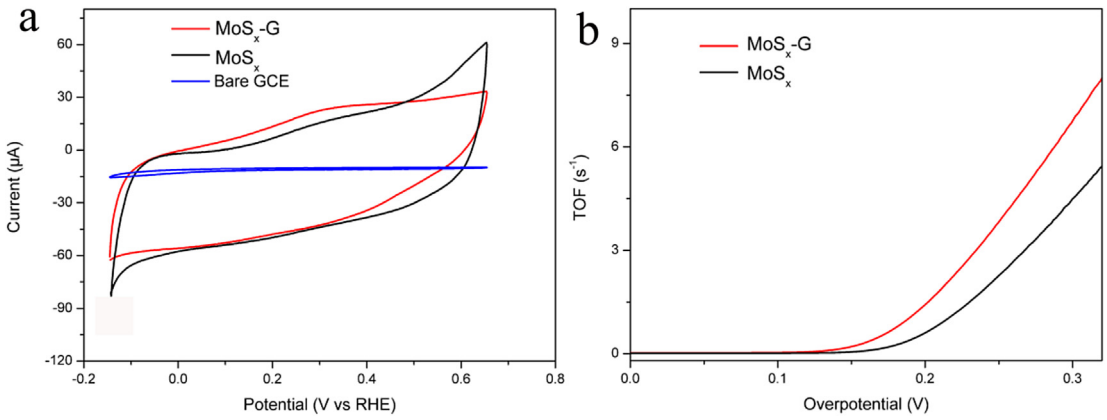

Fig. 4. (a) CVs of MoS_x–G/GCE, MoS_x/GCE and bare GCE recorded in a phosphate buffer solution at pH = 7 and from −0.145 V to 0.655 V vs. RHE with a scan rate of 50 mV s^{-1}. (b) Calculated TOFs for MoS_x–G and MoS_x at 0.5 M H_2SO_4.

4. Conclusions

In summary, simultaneous electrodeposition of MoS_x and graphene from MoS_4^{2-} and GO has been proven to be an effective strategy toward facile deposition of graphene film-confined MoS_x nanoparticles onto electrode surfaces. As a novel HER catalyst, this hybrid film exhibits high activity with an overpotential of 130 mV, a Tafel slope of 43 mV dec^{-1} and good stability. Our present study is important because it provides us a general methodology for simple, one-step fabrication of metal-based nanostructures/graphene hybrid film toward electrocatalysis and other applications.

References

[1] T. Cook, D. Dogutan, S. Reece, Y. Surendranath, T. Teets, D. Nocera, Chem. Rev. 110 (2010) 6474–6502.
[2] M. Dresselhaus, I. Thomas, Nature 414 (2001) 332–337.
[3] M. Walter, E. Warren, J. McKone, S. Boettcher, Q. Mi, E. Santori, N. Lewis, Chem. Rev. 110 (2010) 6446–6473.
[4] Y. Hara, N. Minami, H. Matsumoto, H. Itagaki, Appl. Catal. A 332 (2007) 289–296.
[5] M. Wu, P. Shen, Z. Wei, S. Song, M. Nie, J. Power Sources 166 (2007) 310–316.
[6] J. Greeley, T. Jaramillo, J. Bonde, I. Chorkendorff, J. Nørskov, Nat. Mater. 5 (2006) 909–913.
[7] J. Xie, H. Zhang, S. Li, R. Wang, X. Sun, M. Zhou, J. Zhou, X. Lou, Y. Xie, Adv. Mater. 25 (2013) 5807–5813.
[8] B. Hinnemann, P. Moses, J. Bonde, K. Jørgensen, J. Nielsen, S. Horch, I. Chorkendorff, J. Nørskov, J. Am. Chem. Soc. 127 (2005) 5308–5309.
[9] D. Kong, H. Wang, J. Cha, M. Pasta, K. Koski, J. Yao, Y. Cui, Nano Lett. 13 (2013) 1341–1347.
[10] V.W.H. Lau, A. Masters, A. Bond, T. Maschmeyer, Chem. Eur. J. 18 (2012) 8230–8239.
[11] T. Jaramillo, J. Bonde, J. Zhang, B.L. Ooi, K. Andersson, J. Ulstrup, I. Chorkendorff, J. Phys. Chem. C 112 (2008) 17492–17498.
[12] W. Jaegermann, H. Tributsch, Prog. Surf. Sci. 29 (1988) 1–167.
[13] Y. Li, H. Wang, L. Xie, Y. Liang, G. Hong, H. Dai, J. Am. Chem. Soc. 133 (2011) 7296–7299.
[14] Y. Chang, C. Lin, T. Chen, C. Hsu, Y. Lee, W. Zhang, K. Wei, L. Li, Adv. Mater. 25 (2013) 756–760.
[15] E. Ponomarev, M. Spallart, G. Hodes, C. Clement, Thin Solid Films 280 (1996) 86–89.
[16] L. Chen, Y. Tang, K. Wang, C. Liu, S. Luo, Electrochem. Commun. 13 (2011) 133–137.
[17] V. Koroteev, L. Bulusheva, I. Asanov, E. Shlyakhova, D. Vyalikh, A. Okotrub, J. Phys. Chem. C 115 (2011) 21199–21204.
[18] J. Xiao, X. Wang, X. Yang, S. Xun, G. Liu, P. Koech, J. Liu, J. Lemmon, Adv. Funct. Mater. 21 (2011) 2840–2846.
[19] J. Zabinski, M. Donley, S. Walck, T. Schneider, N. Devitt, Tribol. Trans. 38 (1995) 894–904.
[20] H. Wang, P. Skeldon, G. Thompson, Surf. Coat. Technol. 91 (1997) 200–207.
[21] H. Yu, C. Ma, B. Ge, Y. Chen, Z. Xu, C. Zhu, C. Li, Q. Ouyang, P. Gao, J. Li, Chem. Eur. J. 19 (2013) 5818–5823.
[22] T. Weber, J. Muijsers, J. Niemantsverdriet, J. Phys. Chem. 99 (1995) 9194–9200.
[23] J. Muijsers, T. Weber, R. vanHardeveld, H. Zandbergen, J. Niemantsverdriet, J. Catal. 157 (1995) 698–705.
[24] D. Merki, S. Fierro, H. Vrubel, X. Hu, Chem. Sci. 2 (2011) 1262–1267.
[25] Z. Lu, H. Zhang, W. Zhu, X. Yu, Y. Kuang, Z. Chang, X. Lei, X. Sun, Chem. Commun. 49 (2013) 7516–7918.
[26] S. Trasatti, Electrodes of Conductive Metallic Oxides, Elsevier, New York, 1981.
[27] J. Thomas, Trans. Faraday Soc. 57 (1961) 1603–1611.
[28] B. Conway, B. Tilak, Electrochim. Acta 47 (2002) 3571–3594.
[29] N. Pentland, J.M. Bockris, E. Sheldon, J. Electrochem. Soc. 104 (1957) 182–194.
[30] T. Jaramillo, K. Jørgensen, J. Bonde, J. Nielsen, S. Horch, I. Chorkendorff, Science 317 (2007) 100–102.
[31] Z. Xing, Q. Chu, X. Ren, J. Tian, A. Asiri, K. Alamry, A. Al-Youbi, X. Sun, Electrochem. Commun. 32 (2013) 9–13.